Turkish Journal of Civil Engineering, 2026, 81-104, Paper 838, ***Research Article***

Comparative Evaluation of Arching Mechanisms in Low and High-Rise Embankments

Araz SALIMNEZHAD[1*]
Mostafa ALMASRAF[2*]
Ozer CINICIOGLU[3]
S. Feyza CINICIOGLU[4]

ABSTRACT

Soil arching is a load transfer mechanism that develops due to differential soil movements between adjacent zones, resulting in a redistribution of stresses and a reorganization of the soil structure. This phenomenon plays a critical role in understanding the behavior of piled embankments. A full-scale finite element (FE) modeling approach is employed to investigate the soil arching mechanism, focusing on the identification of compression and extension zones between which force chains of arches are formed along the vertical centerline of the embankment. The coefficient K serves as an indicator of the soil's structural response, enabling the identification of compression and extension zones. A detailed parametric analysis is conducted to assess both Column-Supported (CPS) and Geosynthetic-Reinforced Pile-Supported (GRPS) embankments with different pile spacings and embankment heights. Furthermore, the stress reduction ratio (SRR) of the subsoil within the central pile-to-pile span is evaluated with respect to both embankment height and normalized subsoil settlement. The results reveal that wider pile spacing leads to the formation of higher arches, whereas increased lateral compression near the embankment toes induces larger pile head deflections beneath the shoulder regions. The full-scale modeling approach captures the evolution of arch geometry and stress transfer patterns across the entire embankment, providing valuable insights into the global behavior of piled embankment systems.

Keywords: Soil arching, principal stress directions, lateral earth pressure coefficient (K), soft soils, pile-supported embankments, full-scale embankment finite element model.

Note:
- This paper was received on November 4, 2025 and accepted for publication by the Editorial Board on December 15, 2025.
- Discussions on this paper will be accepted by July 31, 2026.
- https://doi.org/10.18400/tjce.1816915

1 Ozyegin University, Department of Civil Engineering, Istanbul, Türkiye
araz.salimnezhad@ozu.edu.tr - https://orcid.org/0000-0003-3532-8391

2 Ozyegin University, Department of Civil Engineering, Istanbul, Türkiye
mostafa.almasraf@ozyegin.edu.tr - https://orcid.org/0000-0002-9114-6501

3 Bogazici University, Civil Engineering Department, Istanbul, Türkiye
ozer.cinicioglu@bogazici.edu.tr - https://orcid.org/0000-0001-9334-6956

4 Ozyegin University, Department of Civil Engineering, Istanbul, Türkiye
feyza.cinicioglu@ozyegin.edu.tr - https://orcid.org/0000-0002-5380-0832

* These authors contributed equally to this work and share first authorship.

1. INTRODUCTION

Soil arching describes the redistribution of stress within the soil mass due to differential settlement. It was first observed during the construction of military magazine silos in the late 19th century [10]. Terzaghi [31, 32] later explained arching as the transfer of stress from a yielding soil zone to adjacent, less-yielding regions. Since then, soil arching has been recognized as a key factor influencing the performance of embankments, railways, highways, and tunnels [24, 35, 36].

The arching mechanism was first investigated through the classic trapdoor experiments of Terzaghi (1943) [33], which demonstrated that when a portion of the test box base settles, the vertical stress above it decreases while the stresses in the adjacent stationary zones increase, indicating a redistribution of stress. Subsequent studies have improved Terzaghi's simplified assumptions through two- and three-dimensional laboratory studies and analytical models [9, 10, 15, 16, 18, 19, 23]. Modern experiments, including centrifuge modeling [18, 22, 30] and full-scale monitoring [12, 28, 37, 38, 42], have demonstrated that arching evolves progressively and may degrade with large relative displacements. Modern imaging and kinematic techniques have greatly enhanced the resolution in tracking and studying the soil arching. Also, particle image velocimetry [PIV] [20, 29] identifies equal-settlement planes and shear bands without the need for a predefined arch geometry.

Analytical studies generally follow three main approaches: (i) equilibrium-based formulations derived from trapdoor or conduit analogies [6, 18]; (ii) three-dimensional dome or shell models that account for load distribution among piles, reinforcement, and subsoil [16, 19]; and (iii) staged deformation models relating arching ratio to relative displacement via ground-reaction-type curves [9, 11, 14, 18]. These frameworks, though differing in assumptions and simplifications, share the goal of linking subsoil or trapdoor settlement to stress redistribution for design applications.

Numerical modeling has become an essential and complementary approach for investigating soil arching. Finite Element and Finite Difference Methods [1, 2, 24, 25, 27, 34, 40, 43] are capable of capturing large-scale stress–strain behavior and the effects of staged construction, whereas the Discrete Element Method [3, 4, 6, 7, 8, 21, 39] provides insight into the micromechanical behavior and the development of force chains considering interparticle friction and the surface characteristics of both the particles and the testing device.

This paper investigates the soil arching mechanism in piled embankments in both the lateral and vertical directions using finite element analysis. Unlike conventional unit-cell approaches typically employed for analyzing arching behavior, the present study models the entire embankment together with the underlying subsoil, extending laterally. This full-scale configuration allows the development and progression of arching and stress transfer to be examined in both vertical and lateral directions, including the embankment toes where shoulder effects and principal stress rotations are more pronounced. Such a modeling strategy provides a more realistic representation of in-situ behavior, capturing the deformation patterns within both the fill and subsoil in all directions. Consequently, it enables the observation of variations in the arching mechanism and corresponding stress-transfer behavior.

In this study, the behavior of two embankment systems, namely conventional pile-supported (CPS) and geogrid-reinforced pile-supported (GRPS) embankments, was investigated by

considering two height categories for each system: low-rise and high-rise. Embankment height has a significant influence on overall performance because it governs the development of soil arching within the fill due to the stiffness contrast between the piles and the surrounding soil. In CPS embankments, arching develops primarily through soil–pile interaction, whereas in GRPS embankments, the inclusion of a geogrid enhances load transfer and limits differential settlement by reinforcing the fill and modifying the arching geometry.

The formation and height of the arches are controlled by the fill thickness and the pile spacing. The concept of critical embankment height, defined as the minimum height required for the development of full arching, is widely adopted in design. Once full arching occurs, the load of the overlying material is primarily transferred to the piles, thereby minimizing surface settlement. However, the influence of fill height on the overall deformation pattern and the possible variation of arching along the embankment body have not yet been fully addressed.

A series of finite element (FE) analyses were conducted in Plaxis 2D for CPS and GRPS embankments with heights of 4 m and 10 m, representing the low- and high-rise cases, respectively. Using the proposed K-value–based method, the arch height was determined along the mid-span between the central piles. As a novel contribution, the stress reduction ratio (SRR) of the subsoil was evaluated with respect to both embankment height and normalized subsoil settlement. This approach captures the combined effects of increasing fill height and subsoil consolidation on arching efficiency and load transfer to the piles. The pile efficacy and the lateral thrust acting on the pile heads were also analyzed.

The analyses revealed clear differences between the low- and high-rise cases for both CPS and GRPS embankments. For a constant pile spacing, fill height was identified as a key factor controlling the shape and geometry of the developed arches and, consequently, the efficiency of load transfer to the piles. Moreover, the lateral spreading of the embankment and the resulting thrust on the shoulder piles emphasized their critical role in resisting lateral loads, which in some cases exceeded their contribution to vertical load support.

2. NUMERICAL MODEL AND MATERIAL PROPERTIES

The conventional pile-supported (CPS) embankments under self-weight in plane strain 2D conditions were modeled using the finite element method (FEM) based software, Plaxis 2D.

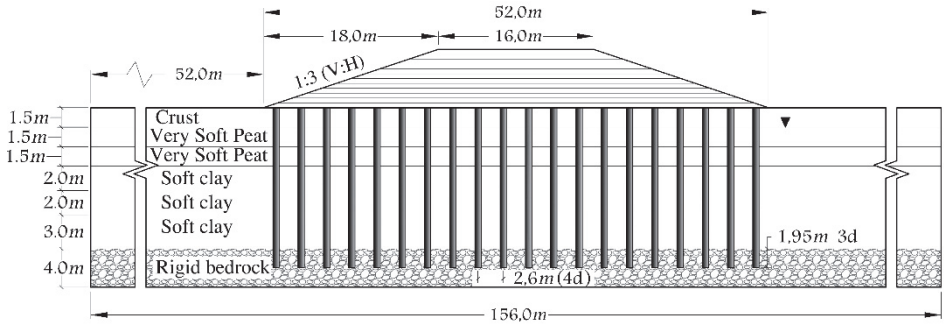

Fig. 1 - Modeled full-scale embankment and sub-soil.

The soil profile of Stanstead Abbots (Willow Plantation or Harlow) was selected as a well-documented case history to represent the soft ground over which the embankment will be constructed [26, 17]. The Stanstead Abbotts embankment was constructed on very soft alluvial deposits with a height of 8.05 m in 274 days. The soil stratigraphy and the validated geotechnical properties of Stanstead Abbotts are presented in Figure 1 and Table 1, respectively. The groundwater table is located at a depth of 1.5 m beneath the ground surface.

Table 1 - Material parameters for the piled embankment.

Material	Soil Model	Unit weight	Poisson's ratio	Permeability	Void ratio	Adopted from Hird et al., 1993		
		γ (kN/m^3)	ν_{ur}	$k_x=k_y$ (m/s)	e_0	λ^*	κ^*	ϕ' (°)
Crust	Soft Soil	16	0.15	2.5×10^{-5}	0.8	0.060	0.009	29
Very soft peat		11.4	0.15	2.5×10^{-5}	7.3	0.147	0.006	34
Very soft peat		11.4	0.15	2.5×10^{-5}	8.2	0.179	0.020	34
Soft clay		16.2	0.15	2.5×10^{-10}	1.5	0.163	0.015	28
Soft clay		16.2	0.15	2.5×10^{-10}	1.45	0.158	0.013	28
Soft clay		16.2	0.15	2.5×10^{-10}	1.4	0.060	0.009	28
Embankment fill	Hardening Soil	19	0.2	4×10^{-5}	0.5	E_{50}^{ref} (kN/m^2)	E_{oed}^{ref} (kN/m^2)	E_{ur}^{ref} (kN/m^2)
						25×10^3	25×10^3	75×10^3
Bedrock	Mohr-Coulomb	27.5	0.3	-	0.5	E'_{ref} (kN/m^2)	-	-
						4.9×10^6		
Pile	Linear Elastic	24	0.3	-	-	30×10^6	-	-

λ^*: modified Cam-Clay compression index, κ^*: modified Cam-Clay swelling index, ϕ': Drained internal friction angle, E_{50}^{ref}: Reference Secant Young's Modulus, E_{oed}^{ref}: Reference Oedometer Modulus, E_{ur}^{ref}: Reference Unloading/Reloading Young's Modulus, E'_{ref}: General Reference Young's Modulus.

The behavior of the soft ground beneath the embankment was modeled using the Soft-Soil Model, which incorporates undrained loading stages followed by consolidation stages in between. Using the soil profile of Stanstead Abbots and adding the piles into the system, two different heights (4 m and 10 m) were considered to analyze the behavior of the GRPS and CPS piled embankments resting on the considered soil profile. The staged construction technique was adopted, and layer placement thicknesses were chosen as 0.5 m each. After completion of fill construction, excess pore water pressure was allowed to dissipate during the final consolidation phase.

The angle of interface friction is taken as 2/3ϕ′ by applying a reduction factor of 2/3 on the shear strength angle of the soil surrounding the piles. The soil profile ends with a bedrock layer at the bottom. Piles of 13.45 meters are embedded for a depth of 3d into the bedrock. The pile diameters (d) are taken as 0.65 m across all models. The center-to-center spacing of the piles varied as 4d, 5d, and 6d. In conventional ground improvement using piles, the design is often expressed through the proportion between the cross-sectional area of the column and the unit cell area, commonly referred to as the area replacement ratio. The area replacement ratio for the 2D embankment models was calculated as 16.67%, 20%, and 25% respectively, for the cases with 6d, 5d, and 4d center-to-center pile spacing. In addition to analyzing CPS embankments, the behavior of GRPS embankments is also examined by adding two layers of geogrid at heights of 0.35 m and 0.70 m above the top of the piles. The geogrid layer is defined as an elastic material with isotropic properties and a stiffness (EA) equal to 1500 kN/m.

Table 2 shows the abbreviated naming system for the embankment models considering their height and center-to-center pile spacing.

Table 2 - The model name abbreviations based on the embankment height and center-to-center pile spacing.

Embankment Height (m)	Center-to-center pile spacing		
	4d (4×0.65 m= 2.6 m)	5d (5×0.65m= 3.25 m)	6d (6×0.65m= 3.9 m)
4	4H-4d	4H-5d	4H-6d
10	10H-4d	10H-5d	10H-6d

Numerical Model Validation

The Stanstead Abbotts embankment was constructed on very soft alluvial deposits and reached a final height of 8.05 m over a period of 274 days. The staged construction sequence (Figure 2) is simulated in the finite element (FE) analysis to accurately replicate the corresponding in-situ loading conditions. The subsurface soil profile was previously modeled by Oztoprak and Cinicioglu (2007) [26] using the Soft Soil Creep and Modified Cam Clay models. As the primary aim of the current study was to investigate the mechanism and evolution of arching, the Soft-Soil model was adopted, taking into account the primary consolidation behavior of the soft soil layers. The soft soil model is based on the Cam-Clay model and is particularly well-suited for modeling normally and lightly over-consolidated clays, silty clays, and peat. The modified swelling and compression indices ($k^*, and\ \lambda^*$) used in the soft soil model differ from their original Cam-Clay counterparts ($k\ and\ \lambda$), described by Burland (1965) [5] as the modified parameters are a function of volumetric strain rather than the void ratio (e), and are given below:

$$\lambda^* = \lambda/(1+e) \quad (1)$$

$$k^* = k/(1+e) \quad (2)$$

The stress-strain response of the subsoil during construction loading was numerically derived and compared with reported stress-strain measurements for the in situ, laboratory Soft Soil Creep model [17], and the Soft Soil Creep model with a revised permeability coefficient (k) [26] for validation purposes. For this comparison, the mid-depths of the second, third, and fourth soil layers (Points a and b in Figure 2) were selected as reference points to evaluate the soft soil model's accuracy in capturing the stress-strain behavior obtained by other soil models and field/laboratory data.

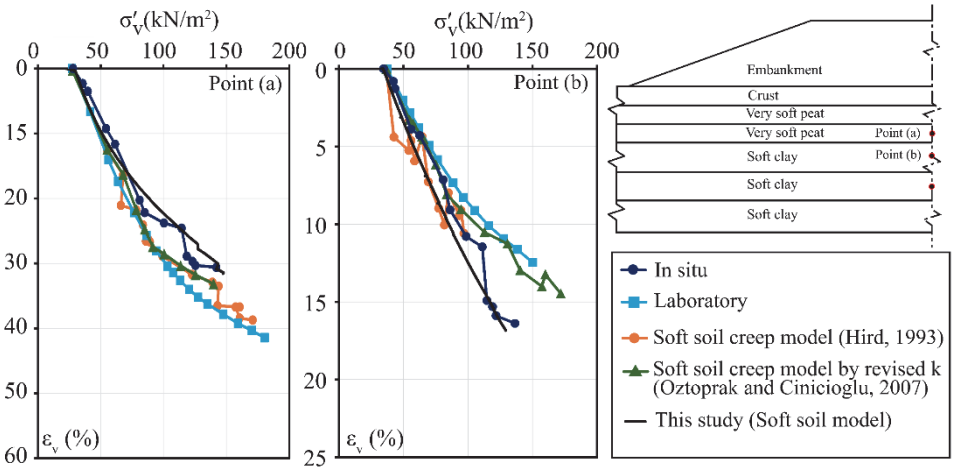

Fig. 2 - Soft-Soil Model validation compared to experimental and numerical data

The validation results are presented in Figure 2. The current numerical modeling approach, incorporating the staged construction conditions and employing the Soft Soil model, exhibited satisfactory agreement with the in-situ observations. The stress-strain results obtained using the Soft Soil model used in this study also showed a good conformance with the other models shown in the comparative graph, thereby confirming the model's reliability and forming the basis for the subsequent simulations conducted in this study.

3. RESULTS AND DISCUSSION

Pile Efficacy as a Measure of the Extent of Arch Evolution

Pile efficacy is defined as the ratio of the load carried by the piles to the total load of the embankment (Eq. 3).

$$E = P/s\gamma H \tag{3}$$

The load on the pile, denoted as "P", represents the total load exerted on the pile. The center-to-center pile distance is shown by "s", "H" is the embankment height, and "γ" is the unit weight of the embankment fill material. To calculate the pile efficacy, first, the load acting on the pile was calculated by taking a horizontal cross-section at the surface of each pile with

a width of 0.65 m, and the acting load along each cross-section was derived. For the calculation of the fill weight at the central part of the embankment, the height of the embankment was taken directly as the full height of the fill at the crest region. In the case of the shoulder regions, the height of the fill was taken as the height of the fill corresponding to the point at the mid-span of the two successive piles. Also, it should be noted that due to the lower height of the 4 m high embankments compared to the 10 m high embankments, they have a narrower base width and a lower number of piles under their base, as seen with fewer piles for the 4 m high embankment in Figure 3.

Figure 3 presents the variation of pile efficacy with respect to pile location for 4 m- and 10 m-high CPS and GRPS embankments. In the case of CPS embankments at the central part of the fill, and for all pile spacings, the 10 m high models have a greater pile efficacy value compared to the 4 m high models, which is expected due to the higher lateral spreading tendency. Moreover, arch heights are reduced by the increase in the embankment height, and the overburden above the level of the arch apices is directly transferred to the piles. As a result, pile efficacy is greater in the case of high-rise embankments. In contrast, arch heights are lower in the case of low-rise embankments. Depending on the spacing of the piles, the arches may not progress up to the full arch state, which may cause a considerable reduction in pile efficacy. In addition to that, due to the small thickness of the overburden above the arch apexes, the load transfer to the piles remains limited, resulting in lower pile efficacy. Even lower pile efficacy values are encountered in the presence of a geogrid layer under low-rise embankments with closely spaced piles. This is due to the restraining effect of the geogrid layer, which reverses the overall mechanism in the lateral direction. Contrary to the case without reinforcement, the regions between the shoulders and the toes are compressed by the restraining effect of the geogrid, thereby increasing the pile efficacy in these regions. The difference between the pile efficacy values of the high-rise and low-rise GRPS embankments in the central section is even more pronounced. Additionally, for the low-rise embankments with pile spacings of 4d and 5d, the GRPS models indicated a lower pile efficacy value in the central regions. Moreover, considering the shoulder region in CPS embankments, for the models with 4d and 5d pile spacings, the 10 m high embankments have greater pile efficacy values compared to the 4 m high cases. It is due to the sharp decrease in the height of the low-rise embankments at the shoulder parts. At the shoulder region of the GRPS embankments, the low-rise and high-rise embankments exhibited almost close values of pile efficacy.

Across all models, the pile efficacy of the central piles is greater for the reinforced models with 10 m heights, and it is even more considerable as the pile spacing increases. This behavior indicates that in larger pile spacings, the geogrid reinforcement gets engaged in a more efficient load transfer to the piles. Also, in all models and all pile spacings, the 10 m high embankments have the highest pile efficacy value. Moreover, the models with the geogrid reinforcement have a higher pile efficacy value compared to their unreinforced counterparts. It is also shown that by approaching the toes, the pile efficacy value decreases for all the models, and these reductions are more intense as the pile spacing increases. In higher embankment heights without reinforcement, the load transfer efficiency is significantly reduced. In the case of low-rise GRPS embankments with 4d and 5d pile spacing, it is obvious that the reinforcement (Figure 3a, b, c).

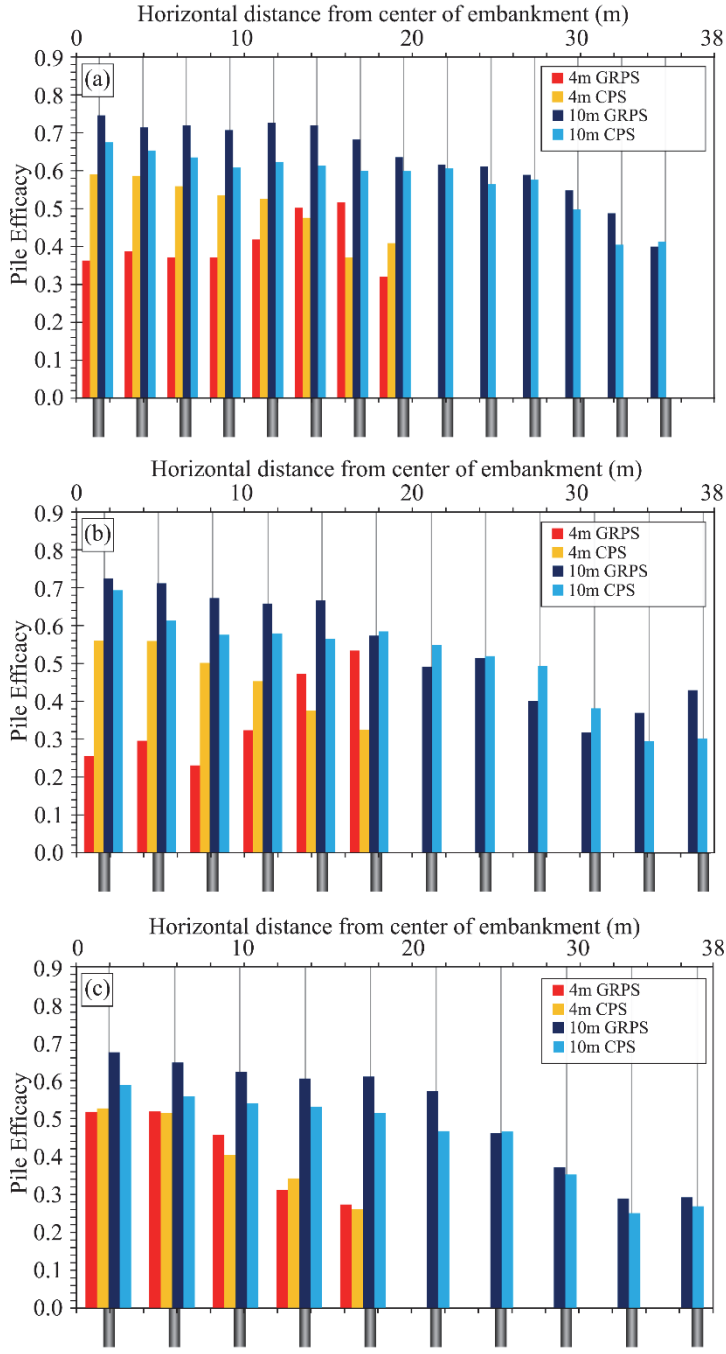

Fig. 3 - Pile efficacy for 4 m and 10 m high CPS and GRPS models with respect to the pile location: (a) 4d pile spacing, (b) 5d pile spacing, and (c) 6d pile spacing

Stress Reduction Ratio (SRR)

In a trapdoor test, the progressive development of the soil arching ratio with respect to the relative displacement of a trapdoor has been identified in both theoretical and experimental studies [14, 18]. This evolution can be represented by a ground reaction curve (GRC), which typically consists of four distinct stages: (i) initial soil arching, (ii) maximum soil arching, corresponding to the minimum soil arching ratio, (iii) stress recovery, and (iv) the ultimate state, corresponding to the ultimate soil arching ratio (Figure 4). However, the same concept of the Ground Reaction Curve (GRC) cannot be directly applied to real embankments.

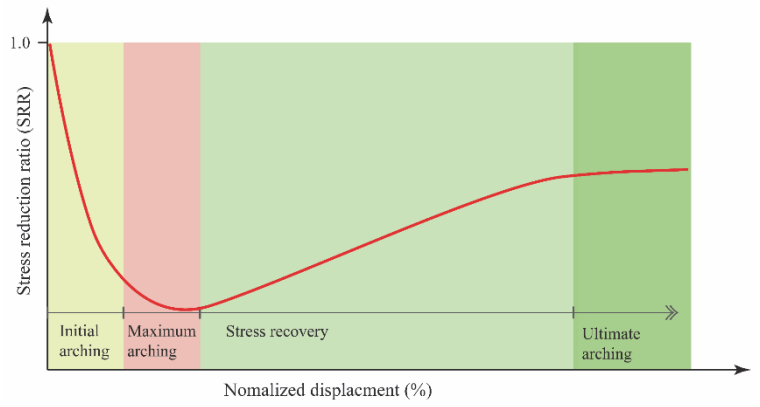

Fig. 4 - SRR versus normalized settlement relationship (adapted from Iglesia et al. 1999, [18]

In a trapdoor test, the trapdoor remains fixed throughout the construction of the fill and is only lowered gradually after the fill has been fully placed, allowing measurement of the acting stresses and corresponding settlements. In contrast, in a real embankment, settlement of the underlying subsoil, analogous to the trapdoor, occurs from the earliest stages of fill placement. Due to this fundamental difference, the shape and evolution of Ground Reaction Curves (GRCs) derived from trapdoor experiments differ significantly from those observed in real embankments. Moreover, while the trapdoor test begins from a fully loaded condition, embankment construction occurs in a staged manner, with the load on the subsoil increasing progressively as each fill layer is placed.

The stress reduction ratio (SRR) is defined as the ratio of the average vertical pressure acting on the subsoil at the clear span between two adjacent piles to the total weight of the soil column above that level [23]. The SRR serves as an indicator of the arching effect, with smaller SRR values reflecting a stronger degree of arching. At the mid-span between the central piles, a stress point and a corresponding node were selected at the surface of the first subsoil layer to record the stress and displacement values throughout the construction process, from the beginning of fill placement to the end of the final consolidation phase. The vertical stress obtained from this point represents the pressure acting on the subsoil, and by considering the embankment height, the SRR was calculated using Equation (4).

$$SRR = \sigma_v/\gamma H \quad (4)$$

Figure 5 illustrates the variation of the stress reduction ratio (SRR) on the subsoil (at the clear spacing between two adjacent piles) versus subsoil settlement (normalized with respect to the clear pile spacing).

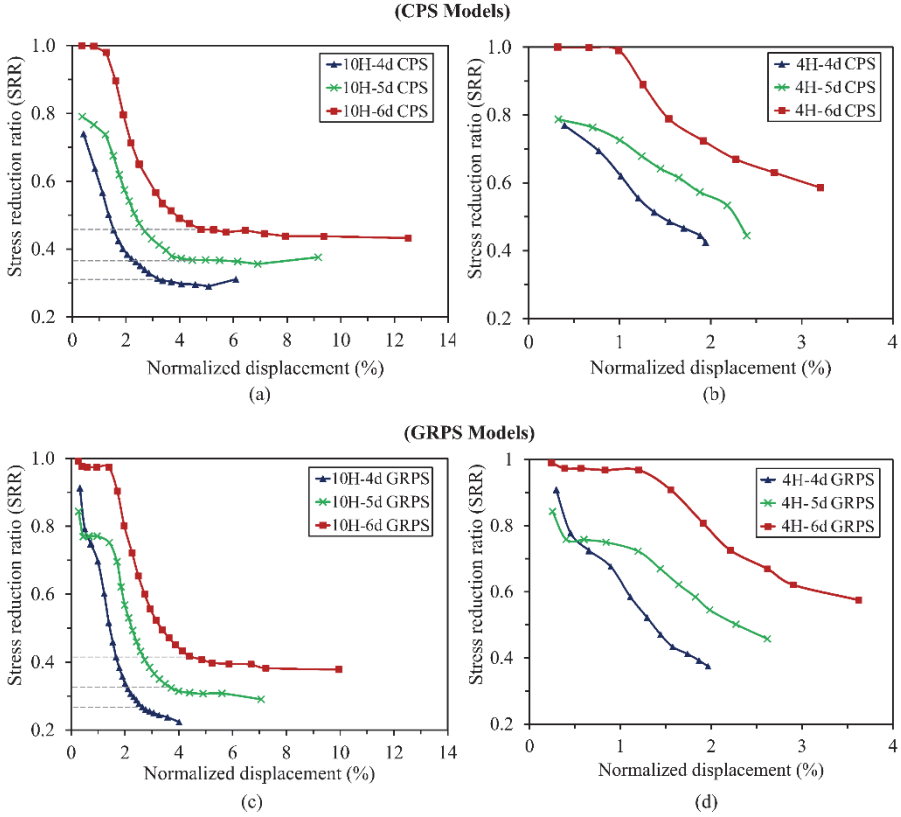

Fig. 5 - SRR values variation at the central sub-soil span versus normalized sub-soil settlement of embankment models with all pile spacings (a) 10 m height CPS, (b) 4 m height CPS, (c) 10 m height GRPS, and (d) 4 m height GRPS

It can be observed that, for the 10 m-high embankments across all pile spacings, the stress reduction ratio (SRR) initially decreases, indicating a progressive enhancement of the arching effect and a greater transfer of load to the piles. Beyond a certain stage, the SRR approaches an almost constant value, showing negligible variation with the subsequent placement of additional fill layers (Figure 5a). In contrast, for the 4 m-high embankments, the stress reduction ratio (SRR) continues to decrease throughout construction and does not reach a constant value by the time the embankment is completed, regardless of the pile spacing (Figure 5b).

This implies that the 4 m-high embankments have not yet achieved the ultimate arching state. If additional fill layers were placed beyond the 4 m height, a further decrease in the stress reduction ratio (SRR) would likely occur. This is because, to maintain a constant crest width with a 1:3 (H:W) shoulder slope ratio, the entire embankment must be constructed with a larger base width. Consequently, as the embankment height increases, each new layer covers a progressively wider area, allowing the embankment to gradually attain the intended overall height and crest width.

For the 10 m-high embankments, the SRR can be regarded as constant, as the construction of additional fill layers does not result in any significant change. In contrast, for the 4 m-high embankments, the SRR curves show no indication of reaching a constant value; instead, they exhibit a continuously decreasing, nearly linear trend. Therefore, no SRR value can be identified as the ultimate value for these lower embankments.

In the case of the GRPS embankments, all models exhibit lower steady-state SRR values, indicating a more effective arching mechanism and, consequently, a more efficient transfer of load to the piles. Additionally, in all GRPS models, the steady-state SRR value was obtained at a greater fill construction height compared to the CPS models (Figure 5c and d). In addition, all 10 m-high GRPS embankments exhibit approximately 2% lower final normalized vertical subsoil settlement compared to the corresponding CPS models.

Lateral Spreading and Pile Deflection

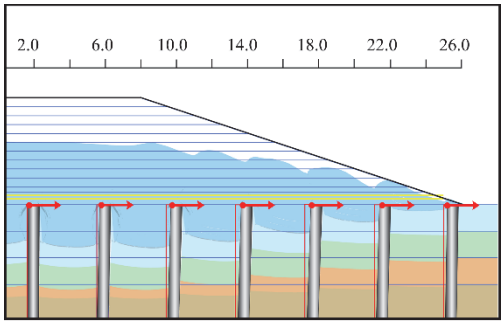

Figure 6 - Lateral deformation of the GRPS model (6m H-6d) and the identified locations of pile head deflection points.

The locations of the pile head for calculating the deflection are illustrated in Figure 6. Figure 7 presents the horizontal pile head deflection observed for the GRPS and CPS embankments with heights of 4m and 10 m, and different pile spacings of 4 d, 5 d, and 6 d. It could be seen that there is a considerable difference between the maximum pile deflections of the GRPS and CPS models. The difference between the deflection of the CPS and GRPS embankment models is more prominent when the center-to-center spacing between the piles increases from 4d (2.6 m) to 6d (3.9 m) (Figure 7a, b, c, and d). This behavior indicates that the maximum

lateral thrust acts on the piles under the mid-shoulders, pushing the head of these piles towards the toe. Also, the effect of the lateral loads on the central piles is negligible.

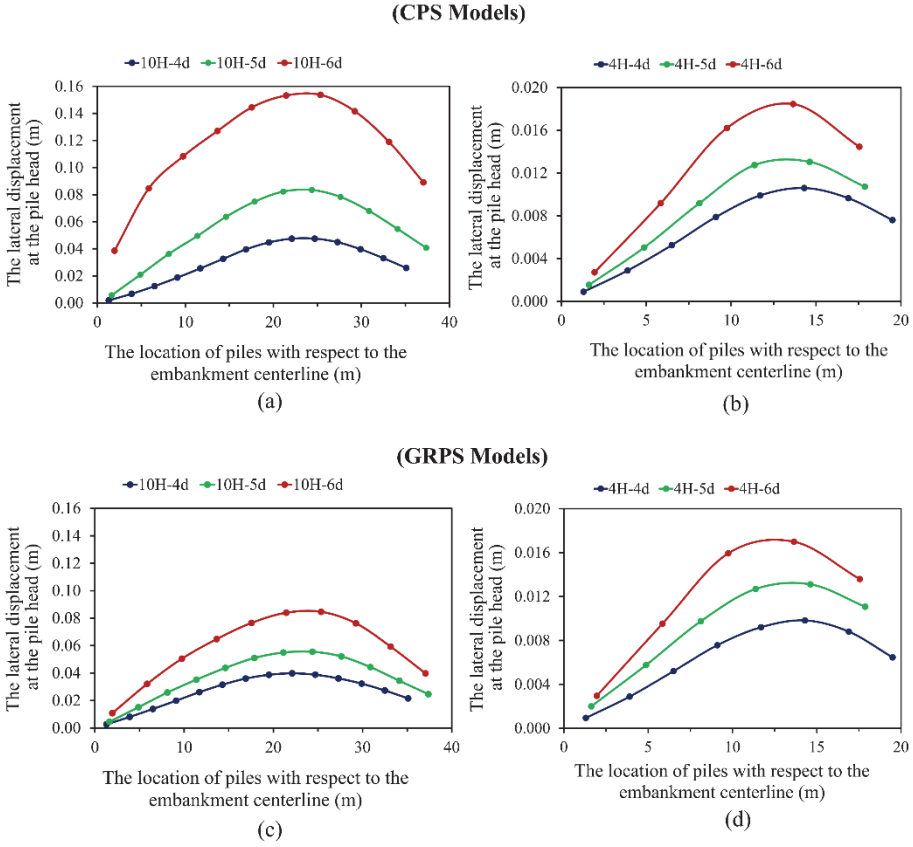

Fig. 7 - Pile head deflection for 10 m and 4 m high CPS and GRPS models

It can be said that the geogrid reinforcement and load transfer platform (LTP) layer effectively contributes to limiting lateral displacements, especially when higher fills and pile spacings are preferred. This limiting effect is more pronounced for the piles located under the shoulders, as the lateral thrust on those piles is at its maximum.

It means that by approaching the toes and under the shoulders, the vertical load over the piles decreases while the lateral load increases, which, along with the lateral spreading of the embankment towards the toes, directs tremendous lateral pressure on the piles located under the shoulders. Under high lateral stress, the piles' heads tend to deflect towards the toes. This deflection is in accordance with the arching behavior above the piles in that region. As the piles get deflected towards the toe, they compress the adjacent soil in the direction of deflection and decompress the adjacent soil opposite to the deflection direction.

There is more than one mechanism that leads to different arching behavior under the shoulders and near the toes. The first mechanism is the classical type of arching that happens under the self-weight of the embankment due to the presence of the piles. However, it should be noted that, unlike the central part of the embankment, the direction of the stress is not vertical under the shoulders. It is due to the slopes of the shoulders, as well as the tendency of the fill material to deform toward the toes from the center. The second behavior is related to the deflection of the piles under the shoulders, which causes arching behavior similar to that behind the retaining walls. In this situation, a part of the fill load is transferred to the side of the pile near the head level. These mechanisms together lead to the formation of the asymmetrical arches with their crown leaning towards the center of the embankment.

Variety of Soil Arching Types

The shape and geometry of the soil arch play a crucial role in governing the redistribution of stress and the sharing of loads between the piles and the subsoil. Among the geometric parameters, the arch height is particularly sensitive to both pile spacing and fill height. In the literature, three primary arching mechanisms are identified: shear-plane arching, partial arching, and full arching [23]. For a given pile spacing, when the embankment height is such that the differential surface settlement of the embankment is nearly equal to the settlement of the subsoil, the mechanism is referred to as shear-plane arching (Figure 8). As the fill height increases and the differential surface settlement becomes smaller than the subsoil settlement, the mechanism transitions to partial arching (Figure 8). Finally, when the embankment height is sufficient for the subsoil settlement to induce almost no differential settlement at the surface, the mechanism is characterized as full arching. Among the three identified arching types, full arching represents the most stable arching structure (Figure 8).

To monitor and evaluate the arching behavior in CPS and GRPS embankments, the variation of the lateral earth pressure coefficient (K) can be examined along a vertical cross-section taken within the fill material at the midspan between the piles. The obtained K-values can be plotted against the embankment height and compared with the theoretical lower and upper bounds (K_a and K_p) to interpret the prevailing stress state of the soil. Additionally, the at-rest earth pressure coefficient (K_0), defined as the ratio of horizontal to vertical stress under the at-rest condition, can be used to distinguish between compression and relaxation zones. Regions where $K > K_0$represent zones dominated by arching, characterized by increased lateral compression above the settling subsoil due to the lateral flow of soil particles from the less-settling areas above the piles and the subsequent development of a jamming effect [18, 24]. Using ranges of K values that denote either extension or compression, all three arching types were successfully identified in the embankment models analyzed in this study. As illustrated in Figure 8, three distinct regions can be identified considering the formed arch in the piled embankments, depending on the fill height and pile spacing: the unloading region (blue), the load transfer region (pink), and the self-weight stress state region (orange). The unloading region includes the arch and the fill beneath it, whose weight is supported by both the piles and the subsoil. The load transfer region serves as the primary pathway through which stresses are transmitted to the piles. In the cases of shear-plane and partial arching, this load transfer region is the only zone, apart from the unloading region, that directly applies load to the piles. In contrast, under full arching conditions, an additional self-weight stress state region develops above the stable arch formation, acting as a surcharge layer. The load

from this region is fully transmitted to the piles through the load transfer region. The interface between the load transfer region and the self-weight stress state region defines the critical embankment height, which is the minimum required height for the formation of a full arch.

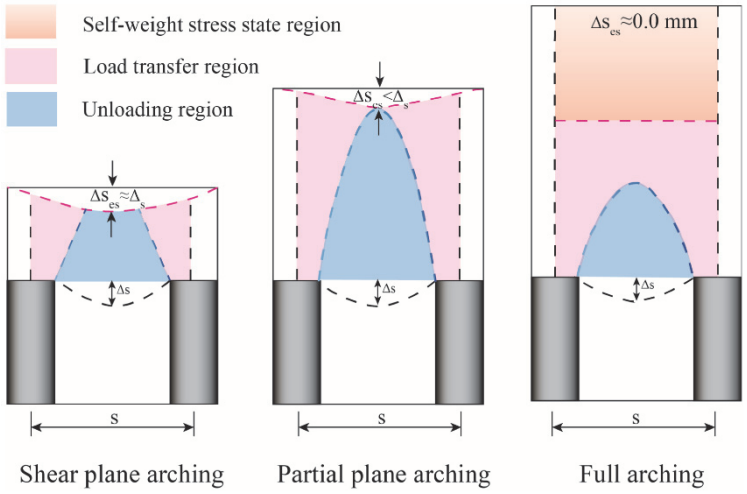

Fig. 8 - Conceptual illustration of possible soil arching structures in pile-supported embankments

Differentiation of Compression and Extension Behaviors within the Embankment

Figure 9 presents the variation of K values with fill height along a vertical cross-section through the centerline of the fill for CPS and GRPS models with embankment heights of 4 m and 10 m. Two distinct ranges of K values can be identified along the cross-section, corresponding to compression (K_p<K<K_0) and relaxation (K_a<K<K_0) zones. For the embankment fill and the Load Transfer Platform (LTP) layer, the theoretical lower and upper bounds of K are $K_a = 0.33, K_p = 3$ and $K_a = 0.26, K_p = 3.852$, respectively. The results indicate that a full arching mechanism is mobilized in all 10 m high CPS and GRPS models within the analyzed span (Figure 9a and c) [21, 41].

A generalized arch height or plane of equal settlement height cannot be distinctly defined in piled embankments by considering only a single pile-to-pile span or focusing exclusively on the central span. This is because settlement patterns and arching mechanisms are not isolated phenomena; rather, they are mutually interactive across adjacent spans, influencing one another through the continuity of the fill and the geosynthetic reinforcement. The shoulder regions of the embankment exhibit a markedly different response compared to the central zone. As the fill material spreads laterally, these regions undergo additional horizontal compression, leading to the development of localized arching mechanisms directed toward the embankment toes. Moreover, the horizontal stress distribution along the base of the embankment typically reaches its maximum near the mid-slope, where significant lateral thrust acts on the sides of the piles. This lateral pressure induces bending of the pile heads

toward the toes, producing deformation patterns analogous to those observed in retaining wall behavior. (Horizontal stress patterns and principal stress directions patterns).

The arch heights, determined from the variation of K values along the central section of the embankment are summarized in Tables 3 and 4 for the CPS and GRPS embankments, respectively. In the case of 4d pile spacing, the arch height shows little sensitivity to increases in embankment height. However, for the 5d and 6d configurations, an increase in embankment height results in a noticeable reduction in arch height. As expected, the arch height increases with wider pile spacing. Moreover, for lower embankment height, variations in pile spacing exert a stronger influence on the extent of arch expansion. All GRPS models have a greater arch height compared to the CPS models due to the presence of the geogrid and LTP layer.

As illustrated in Figure 9, the compression zone serves as a key indicator of the arching mechanism and the mobilized shear strength within the embankment. The thickness of this compression region increases with greater pile spacing. The most highly compressed portion of the arch corresponds to the location where the K value approaches $K_p = 3$. As the embankment spreads laterally from the centerline toward the toes, a relaxation zone develops, characterized by K values ranging between K_0 and K_a (Figure 9a and b). In the GRPS models, however, the height of the relaxation zone is notably smaller than in the CPS embankments. The inclusion of geogrid reinforcement constrains horizontal deformation, thereby reducing the extent of the relaxation zone (Figure 9c and d).

At the central part of the embankment (beneath the crest), the fill material above the arch domes tends to move laterally toward the sides of the arch apex. This occurs because the arch zones are relatively stiffer, redirecting the overlying soil mass. As a result, the overburden load is not carried entirely by the piles; instead, part of it is transferred to the piles, while the rest is diverted toward the embankment toes (see Figure. 10). This observation differs from the findings of Van Eekelen [35, 36], who suggested that the full load above the arches is borne by the piles. In contrast, the present study shows that only part of the load is transferred directly to the piles, with a portion redistributed laterally toward the toes.

The unreinforced piled embankments with a height of 4 m exhibit a behavior similar to that of the 10 m high models. However, as the pile spacing increases, the arching mechanism transitions from full arching in the 4d and 5d cases to partial arching in the 6d configuration, where the arch height becomes nearly equal to the fill height (Figure 9b) [21]. In the reinforced models, a sharp increase in K values are observed at the interface between the fill and the Load Transfer Platform (LTP) layer (at a height of approximately 1 m), which is a natural consequence of the higher internal friction angle and stiffness of the LTP layer compared to the surrounding fill soil.

The Load Transfer Platform (LTP) layer has a thickness of 1 m and is reinforced with two geogrid layers placed at 0.35 m and 0.70 m above the pile heads. The upper portion of the LTP layer undergoes greater compression than the lower portion due to the sagging behavior of the LTP layer. The compressive stresses are resisted by the LTP material itself, while the lower geogrid layer mobilizes tensile resistance within the tension zone. This flexural-type mechanism predominates in the zones between the piles, whereas an inverse stress distribution is observed directly above the pile heads, where the compressive and tensile regions are interchanged [13].

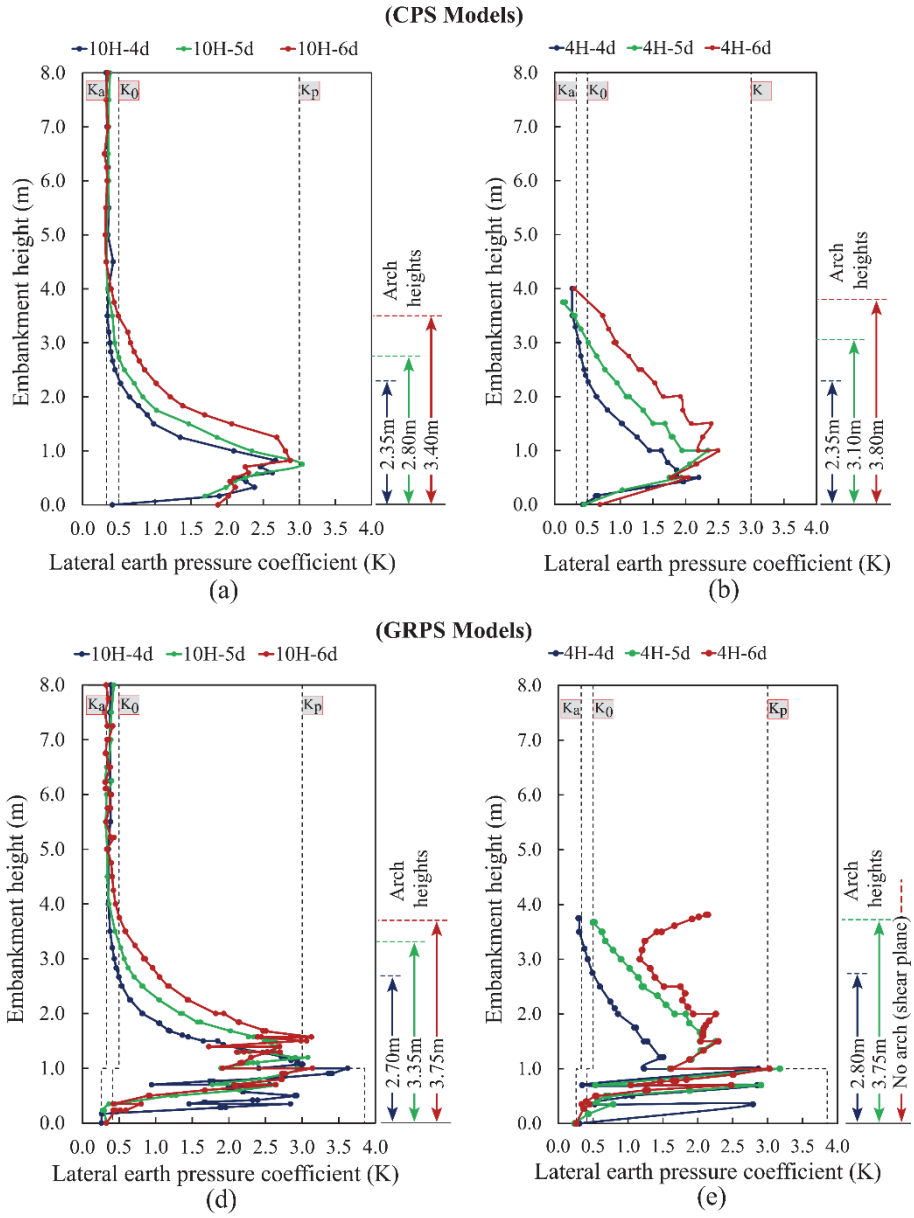

Fig. 9 - K value variation along the vertical cross-section at the centerline of embankments with 4d, 5d, and 6d pile spacings: (a) 10 m high CPS embankments; (b) 4 m high CPS embankments; (c) 10 m high GRPS embankments, and (d) 4 m high GRPS embankments

In the non-reinforced embankments with a height of 4 m, full arching was observed for pile spacings of 4d and 5d, while partial arching developed at a spacing of 6d. For the GRPS

models, the identified arch types were full arching, partial arching, and shear-plane arching corresponding to the 4d, 5d, and 6d pile spacings, respectively [21] (Tables 3 and 4).

Table 3 - Determined arch height for the CPS embankments using the K value variation.

CPS Model Height (m)	Pile Spacing		
	4d	5d	6d
	Arch Height (m)		
4	2.35	3.1	3.8
10	2.35	2.8	3.4

Table 4 - Determined arch height for the GRPS embankments using the K value variation.

GRPS Model Height (m)	Pile Spacing		
	4d	5d	6d
	Arch Height (m)		
4	2.8	3.75	-
10	2.7	3.35	3.75

Horizontal Displacement Contours and the Behavior of the Embankments

The horizontal displacement contours for the 10H-5d and 4H-5d CPS and GRPS embankments are presented in Figure 10. These contours illustrate the cumulative horizontal displacements within the embankment body from the beginning of construction to the completion of the final consolidation phase. The 5d pile spacing cases were selected as representative of the average spacing among the models analyzed in this study. As shown in Figures 10a and b, for both the 10H–5d CPS and GRPS embankments, horizontal displacement increases noticeably beneath the shoulders and toward the embankment toes. This indicates a deformation pattern extending from the centerline toward the toes, referred to as lateral spreading of the embankment. Such deformation is responsible for the relaxation behavior observed in the K-value variations near the central part of the fill. A comparison between the 10 m-high CPS and GRPS models shows that the inclusion of geogrid reinforcement effectively restrains and limits the lateral spreading of high embankments. In contrast, the horizontal displacement patterns of the low-rise (4 m high) CPS and GRPS embankments display similar deformation behavior (Figure 10c and d). This occurs because the lighter weight of the low-rise fills is insufficient to fully mobilize the geogrid layers, unlike in the heavier 10 m high embankments. Furthermore, in the case of the 4H–5d GRPS embankment, the arching mechanism can be classified as partial arching, meaning that the arch height is nearly equal to the embankment height. This condition results in a less efficient load transfer to the piles and leads to comparatively larger horizontal and vertical displacements than those observed in the corresponding 4H-5d CPS model.

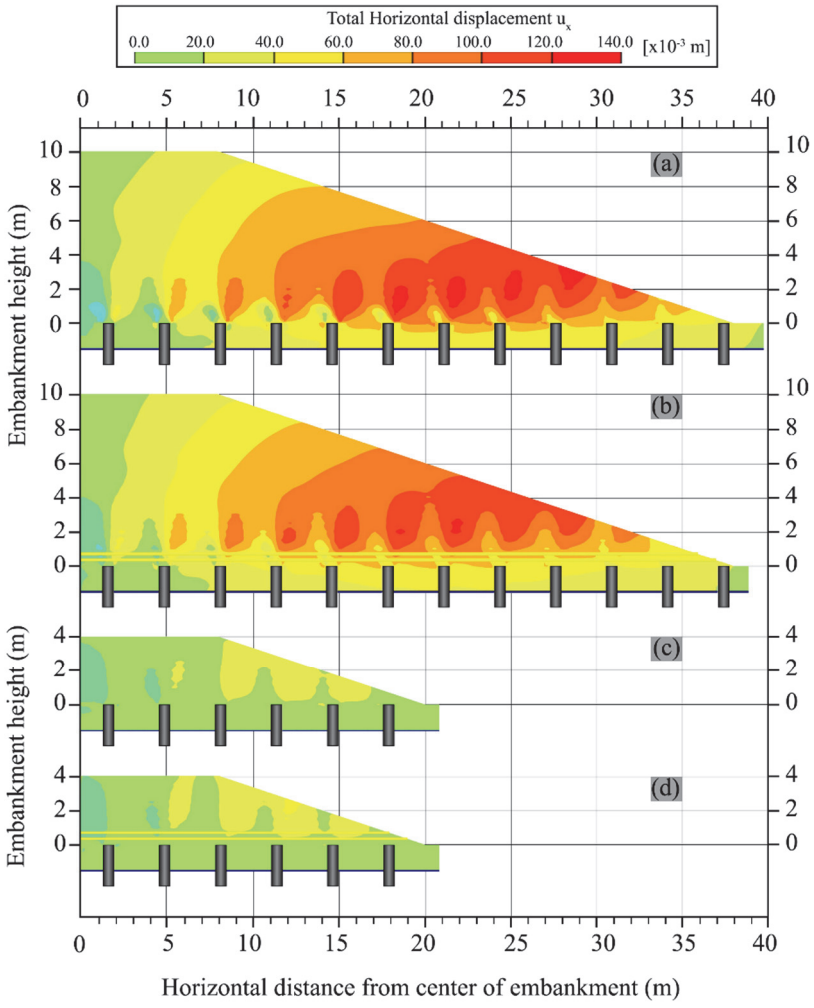

Fig. 10 - The horizontal displacement contours of embankment models: (a) 10H-5d CPS, (b) 10H-5d GRPS, (c) 4H-5d CPS, and (d) 4H-5d GRPS

Principal Stress Directions

The arching and compression zone can also be demonstrated by tracking principal stress directions because the arching mechanism is inherently associated with principal stress rotation. The principal stress directions of 10H-4d and 4H-4d CPS models are shown in Figure 11, at the center, mid-slope, and toe regions.

In the case of the 10H-4d CPS embankment model, at the center of the fill, the principal stress directions above the subsoil exhibit a rotation towards a horizontal orientation at a specific height, approximately 1.5 m above the subsoil centerline (Figure 11a), forming an arched

zone that supports the overlying fill mass. The central arch exhibits symmetrical geometry, as indicated by the dashed lines representing shear bands that extend from the corners of the central piles (Figure 11a).

In the mid-slope region, approximately corresponding to the midpoint of the inclined fill shoulder, the inclined nature of the soil loading causes the major principal stress directions to deviate from vertical alignment above the arching zone. Consequently, the angles formed between the shear band trajectories (arch feet) and the pile heads differ between the adjacent left and right piles, resulting in an asymmetrical, parabolic arch geometry (Figure 11b). Near the toe of the embankment, the principal stress directions become nearly parallel to the slope of the shoulder, leading to insufficient overlap of stress trajectories and preventing the formation of a distinct arch structure (Figure 11c).

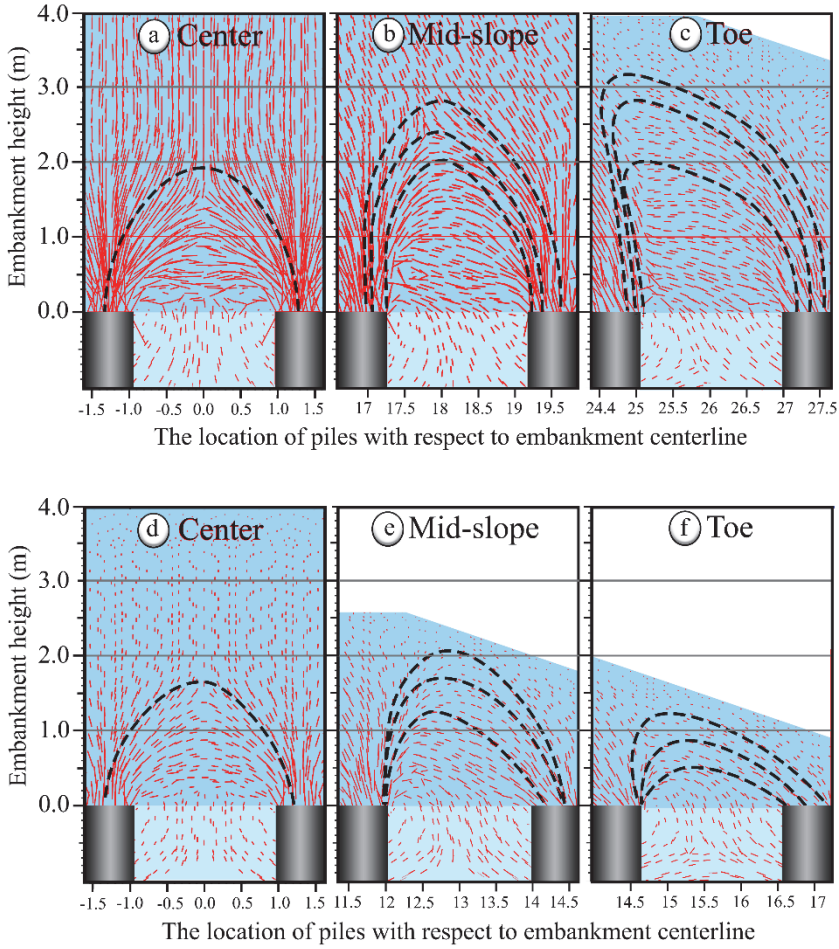

Fig. 11 - The principal stress directions of CPS models: (a), (b), (c)10H-4d and (d), (e), (f) 4H-4d

Considering the 4H-4d CPS models, a similar behavior can be observed in comparison to the 10H-4d CPS model regarding the principal stress directions (Figure 11d). The main differences can be observed in the principal stress directions pattern at the mid-slope and toe parts, where, due to the insufficient height of the fill in these regions, the principal stress bands are almost extended up to the surface of the embankment (Figure 11e and f). All in all, the results indicate that due to lateral spreading and changes in embankment height at the slopes, different arching types form along the body of the embankment. Moreover, the arches under the shoulders and close to the toes could not be considered geometrically symmetric due to the inclination of the slopes and the concentration of the lateral stresses at those regions.

4. CONCLUSION

Piled embankments over soft soils transfer the majority of their imposed loads to the piles through the soil arching mechanism. Arching develops as a consequence of the structuration and restructuration processes occurring within the embankment body, where the loads are diverted from more yielding zones toward less yielding ones. This differential movement results in the formation of stress arches, enabling a progressive concentration of loads onto the pile heads while reducing stress transmission to the underlying soft ground. The degree of arching mobilization is governed by several factors, including the embankment height, pile spacing, the stiffness contrast between the piles and the intervening soil, and the ability of the reinforcement layer, if present, to restrain lateral spreading. When geogrid reinforcement is incorporated, it contributes to the overall load transfer by mobilizing tensile membrane action and by stabilizing the upper soil layers, thereby enhancing the efficiency of arch formation. Consequently, the combined effects of soil arching and reinforcement interaction lead to reduced differential settlements, improved stability, and a more uniform stress distribution throughout the embankment.

The formation and height of the arches are controlled by the thickness of the fill and the spacing of the piles. Additionally, depending on the embankment height and pile spacing, the arch formation may not progress to the full arching state. Three states can be pronounced as: shear plane arching, partial plane arching, and full arching, each of which is connected with different load transfer and settlement mechanisms. To analyze and disclose the main features of this significant distinction into account, this study analyzes the behavior of full-scale embankments with two different heights, one representing the low-rise embankments (4 meters in height), and the other representing the high-rise embankments (10 meters in height), with three different pile spacings for each of them.

The findings of this study provide quantitative insight into the evolution and distribution of soil arching within full-scale piled embankments, both high-rise and low-rise, considering both the conventional piled embankments (CPS) and geogrid-reinforced piled embankments (GRPS). Therefore, the findings of this paper offer a robust framework for interpreting the interaction between embankment geometry, reinforcement efficiency, and load transfer mechanisms.

Acknowledgements

The authors would like to thank the Scientific and Research Council of Turkey [TUBITAK] for supporting this study with project number 122M040.

Statements and declarations

Data availability

Some or all data supporting this study's findings are available from the corresponding authors upon reasonable request.

Declaration of Competing Interest

The authors declare that they have no known competing financial interests or personal relationships that could have appeared to influence the work reported in this paper.

References

[1] Al-Naddaf M, Han J, Xu C, Jawad S, Abdulrasool G. Experimental investigation of soil arching mobilization and degradation under localized surface loading. J Geotech Geoenviron Eng 2019;145(12):04019114. https://doi.org/10.1061/(ASCE)GT.1943-5606.0002190

[2] Başar EE, Çelik İD, Fındık M, Uzundurukan S. Kohezyonsuz zeminde kazık aralığının belirlenmesi ve temel davranışının deneysel incelenmesi (In Turkish). Turkish Journal of Civil Engineering. 2023 Mar;34(2):145-72. https://doi.org/10.18400/tjce.1244594

[3] Bathurst RJ, Rothenburg L. Micromechanical aspects of isotropic granular assemblies with linear contact interactions. Géotechnique 1988;38(1):19-39. https://doi.org/10.1115/1.3173626

[4] Bhandari A, Han J. Investigation of geotextile-soil interaction under a cyclic vertical load using the discrete element method. Geotext Geomembr 2010;28(1):33-43. https://doi.org/10.1016/j.geotexmem.2009.09.005

[5] Burland JB. The yielding and dilation of clay. Géotechnique 1965;15(1):211-214. https://doi.org/10.1680/geot.1965.15.2.211

[6] Chevalier B, Combe G, Villard P. Experimental and discrete element modeling studies of the trapdoor problem: influence of the macro-mechanical frictional parameters. Acta Geotech 2012;7(1):15-39. https://doi.org/10.1007/s11440-011-0152-5

[7] Chevalier B, Combe G, Villard P. Experimental and numerical studies of load transfers and arching effect. Proc 12th Int Conf Int Assoc Comput Adv Geomech (IACMAG), Goa, India, 2008, pp. 273-280.

[8] Cundall PA, Strack OD. A discrete numerical model for granular assemblies. Géotechnique 1979;29(1):47-65. https://doi.org/10.1680/geot.1979.29.1.47

[9] Feda J, Boháč J, Herle I. Physical similitude and structural collapse in K_0 compression of soils. J Geotech Eng 1995;121(2):210-215. https://doi.org/10.1061/(ASCE)0733-9410(1995)121:2(210)

[10] Feld J. Early history and bibliography of soil mechanics. Proc 2nd Int Conf Soil Mech Found Eng, Rotterdam, Netherlands, 1948, Vol 1, pp. 1-7.

[11] George TI, Dasaka SM. Mechanics of arch action in soil arching. Acta Geotech 2023;18(4):1991-2009. https://doi.org/10.1007/s11440-022-01697-0

[12] Ghosh B, Fatahi B, Khabbaz H, Nguyen HH, Kelly R. Field study and numerical modelling for a road embankment built on soft soil improved with concrete-injected columns and geosynthetic-reinforced platform. Geotext Geomembr 2021;49(3):804-824. https://doi.org/10.1016/j.geotexmem.2020.12.010

[13] Ghosh B, Fatahi B, Khabbaz H, Yin JH. An analytical study for a double-layer geosynthetic reinforced load transfer platform on a column improved soft soil. Geotext Geomembr 2017;45(5):508–536. https://doi.org/10.1016/j.geotexmem.2017.06.006

[14] Han J, Wang F, Al-Naddaf M, Xu C. Progressive development of two-dimensional soil arching with displacement. Int J Geomech 2017;17(12):04017112. https://doi.org/10.1061/(ASCE)GM.1943-5622.0001025

[15] Handy RL. The arch in soil arching. J Geotech Eng 1985;111(3):302-318. https://doi.org/10.1061/(ASCE)0733-9410(1985)111:3(302)

[16] Hewlett WJ, Randolph MF. Analysis of piled embankments. Int J Rock Mech Min Sci Geomech Abstr 1988;25(6):297-298. https://doi.org/10.1016/0148-9062(88)91283-1

[17] Hird CC, Pyrah IC, Russell D, Cinicioglu FJC. Modelling the effect of vertical drains in two-dimensional finite element analyses of embankments on soft ground. Can Geotech J 1995;32(5):795-807. https://doi.org/10.1139/t95-077

[18] Iglesia GR, Einstein HH, Whitman RV. Investigation of soil arching with centrifuge tests. J Geotech Geoenviron Eng 2014;140(2):04013005. https://doi.org/10.1061/(ASCE)GT.1943-5606.0000998

[19] Kempfert H, Göbel C, Alexiew D, Heitz C. German recommendations for reinforced embankments on pile-similar elements. Proc EuroGeo3 Conf Geotech Eng with Geosynthetics, Munich, Germany, 2004, pp. 279-284.

[20] Khatami H, Deng A, Jaksa M. An experimental study of the active arching effect in soil using the digital image correlation technique. Comput Geotech 2019;108:183-196. https://doi.org/10.1016/j.compgeo.2018.12.023

[21] Lai HJ, Zheng JJ, Zhang RJ, Cui MJ. Classification and characteristics of soil arching structures in pile-supported embankments. Comput Geotech 2018;98:153-171. https://doi.org/10.1016/j.compgeo.2018.02.007

[22] Liu H, Luo Q, El Naggar MH, Zhang L, Wang T. Centrifuge modeling of stability of embankment on soft soil improved by rigid columns. J Geotech Geoenviron Eng 2023;149(9):04023069. https://doi.org/10.1061/JGGEFK.GTENG-11314

[23] McNulty JW. An experimental study of arching in sand. Univ Illinois Urbana-Champaign, 1965.

[24] Meena NK, Nimbalkar S, Fatahi B, Yang G. Effects of soil arching on behavior of pile-supported railway embankment: 2D FEM approach. Comput Geotech 2020;123:103601. https://doi.org/10.1016/j.compgeo.2020.103601

[25] Okyay US, Dias D. Use of lime and cement treated soils as pile-supported load transfer platform. Eng Geol 2010;114(1-2):34-44. https://doi.org/10.1016/j.enggeo.2010.03.008

[26] Oztoprak S, Cinicioglu SF. Looking into an appropriate methodology for the embankment design and construction on soft soils. Lowland Technol Int 2007;9(2):21-28.

[27] Oztoprak S, Cinicioglu SF. Soil behaviour through field instrumentation. Can Geotech J 2005;42(2):475-490. https://doi.org/10.1139/t04-121

[28] Pan G, Liu X, Yuan S, Wang Y, Sun D, Feng Y, Jiang G. A field study on the arching behavior of a geogrid-reinforced floating pile-supported embankment. Transp Geotech 2022;37:100795. https://doi.org/10.1016/j.trgeo.2022.100795

[29] Rui R, Zhai YX, Han J, Van Eekelen SJM, Chen C. Deformations in trapdoor tests and piled embankments. Geosynth Int 2020;27(2):219-235. https://doi.org/10.1680/jgein.19.00014

[30] Shen P, Xu C, Han J. Centrifuge tests to investigate global performance of geosynthetic-reinforced pile-supported embankments with side slopes. Geotext Geomembr 2020;48(1):120-127. https://doi.org/10.1016/j.geotexmem.2019.103527

[31] Smith EJ, Bouazza A, King LE, Rowe RK. New insights into soil arching behavior in column-supported embankments. Can Geotech J 2022;59(6):901-921. https://doi.org/10.1139/cgj-2021-0186

[32] Terzaghi K. Stress distribution in dry and in saturated sand above a yielding trapdoor. Harvard Univ Eng Exp Station Publ 1936;99:1-11.

[33] Terzaghi K. Theoretical soil mechanics. John Wiley & Sons, New York, 1943, pp. 11-15. https://doi.org/10.1002/9780470172766

[34] Van der Peet TC, Van Eekelen SJM. 3D numerical analysis of basal reinforced piled embankments. Proc 10th Int Conf Geosynthetics, Berlin, Germany, 2014.

[35] Van Eekelen SJ, Bezuijen A, Lodder HJ, Van Tol AF. Model experiments on piled embankments. Part I. Geotext Geomembr 2012;32:69-81. https://doi.org/10.1016/j.geotexmem.2011.11.002

[36] Van Eekelen SJ, Bezuijen A, Lodder HJ, Van Tol AF. Model experiments on piled embankments. Part II. Geotext Geomembr 2012;32:82-94. https://doi.org/10.1016/j.geotexmem.2011.11.003

[37] Wang G, Zhang X, Liu X, Wang H, Xu L, Liu H, Peng L. Soil arching effect in reinforced piled embankment for motor-racing circuit: field tests and numerical analysis. Transp Geotech 2022;37:100844. https://doi.org/10.1016/j.trgeo.2022.100844

[38] Wang T, Ma H, Liu K, Luo Q, Xiao S. Load transfer and performance evaluation of piled beam-supported embankments. Acta Geotech 2022;17(9):4145-4171. https://doi.org/10.1007/s11440-022-01519-3

[39] Wang Z, Jacobs F, Ziegler M. Visualization of load transfer behaviour between geogrid and sand using PFC2D. Geotext Geomembr 2014;42(2):83-90. https://doi.org/10.1016/j.geotexmem.2014.01.001

[40] Wijerathna M, Liyanapathirana DS. Load transfer mechanism in geosynthetic-reinforced column-supported embankments. Geosynth Int 2020;27(3):236-248. https://doi.org/10.1680/jgein.19.00022

[41] Ye GB, Wang M, Zhang Z, Han J, Xu C. Geosynthetic-reinforced pile-supported embankments with caps in a triangular pattern over soft clay. Geotext Geomembr 2020;48(1):52-61. https://doi.org/10.1016/j.geotexmem.2019.103504

[42] Zhang C, Su L, Jiang G. Full-scale model tests of load transfer in geogrid-reinforced and floating pile-supported embankments. Geotext Geomembr 2022;50(5):896-909. https://doi.org/10.1016/j.geotexmem.2022.05.004

[43] Zhuang Y, Wang K. Finite element analysis on the dynamic behavior of soil arching effect in piled embankment. Transp Geotech 2018;14:8-21. https://doi.org/10.1016/j.trgeo.2017.09.001